

Supplementary data

Structure-evolved YbBiO₃ perovskite for highly formate-selective CO₂ electroreduction

Jiaying Yan^a, Xuanyu Wang^a, Yayu Guan^a, Yuyu Liu^{a,*}, Linlin Wang^a, Qinsi Shao^{a,*}, and
Qiu Huang^a

^a Institute for Sustainable Energy, College of Sciences, Shanghai University, Shangda Road
99, Baoshan, Shanghai 200444, China

E-mail: liuyuyu@shu.edu.cn; liuyuyu2014@126.com

Content

Fig. S1. Schematic illustration of the material synthesis process.

Fig. S2. (a) XRD pattern of Bi₂O₃ NPs, SEM images of (b) Bi₂O₃ NPs, (c) Bi₂O₃ NPs after electroreduction.

Fig. S3. LSV curves of Bi₂O₃ NPs, YBO@600 and YBO@800 in 0.1M KHCO₃ saturated with Ar.

Fig. S4. (a) FE_{CO} diagram of Bi₂O₃ NPs, YBO@600 and YBO@800 at varied applied potentials. (b) FE_{H_2} of Bi₂O₃ NPs, YBO@600 and YBO@800 at varied applied potentials.

Fig. S5. Current density of Bi₂O₃ NPs, YBO@600 and YBO@800 at varied applied potentials.

Fig. S6. The $FE_{formate}$ and current density during the stability test of Bi₂O₃ NPs in H-type cell at -0.9 V_{RHE}.

Fig. S7. XRD pattern of YBO@800 catalyst after 80h stability test.

Fig. S8. Installation diagram of flow-cell.

Fig. S9. Pictures of flow-cell system.

Fig. S10. LSV curve of the YBO@800 catalyst in the flow-cell with CO₂ injection.

Fig. S11. The $FE_{formate}$ and current density of the YBO@800 catalyst at different potentials in the flow-cell.

Fig. S12. (a) XRD pattern of YBO@600, SEM images of (b) YBO@600, (c) YBO@600 after electroreduction.

Fig. S13. Yb 4d XPS spectra of YBO@800 and e-YBO.

Fig. S14. CV curves of the catalysts at different sweep speeds: (a) YBO@800, (b) e-YBO.

Fig. S15. (a) N₂ adsorption–desorption isotherms of YBO@800, (b) e-YBO. (c) BET surface area of YBO@800 and e-YBO.

Fig. S16. EIS plots of Bi₂O₃ NPs and YBO@600.

Table. S1. Inductively Coupled Plasma Optical Emission Spectrometer (ICP-OES) results for mole ratio of Bi and Yb in YBO@800.

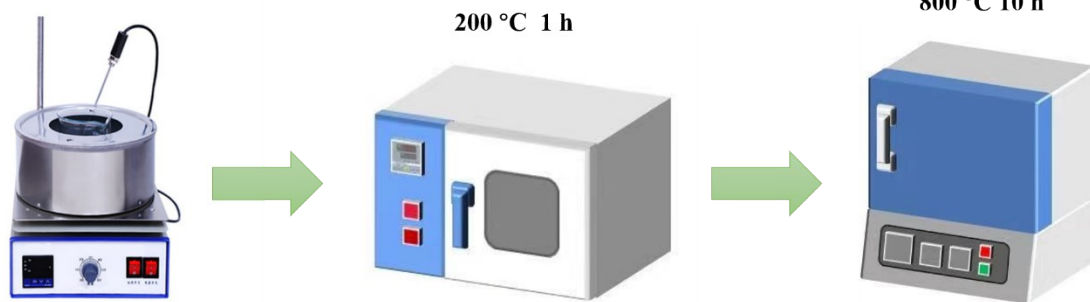
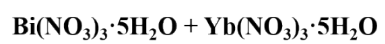


Fig. S1. Schematic illustration of the material synthesis process.

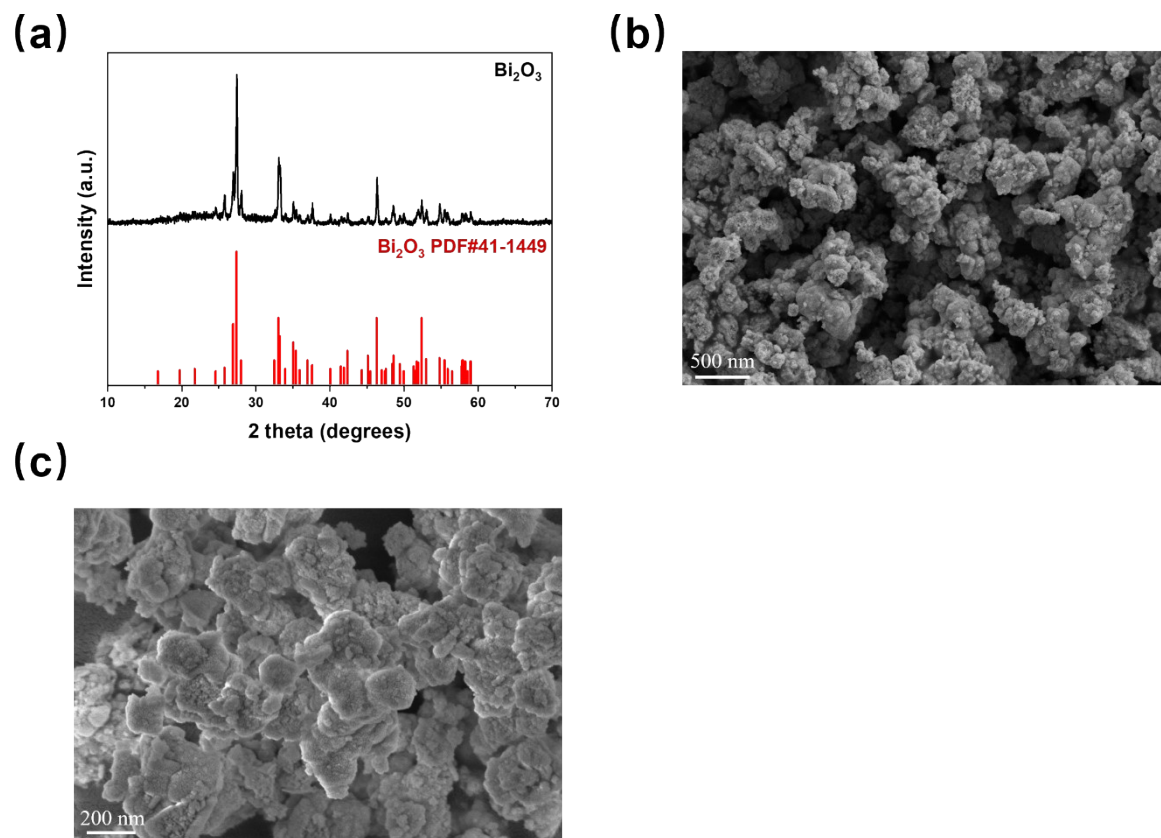


Fig. S2. (a) XRD pattern of Bi_2O_3 NPs, SEM images of (b) Bi_2O_3 NPs, (c) Bi_2O_3 NPs after electroreduction.

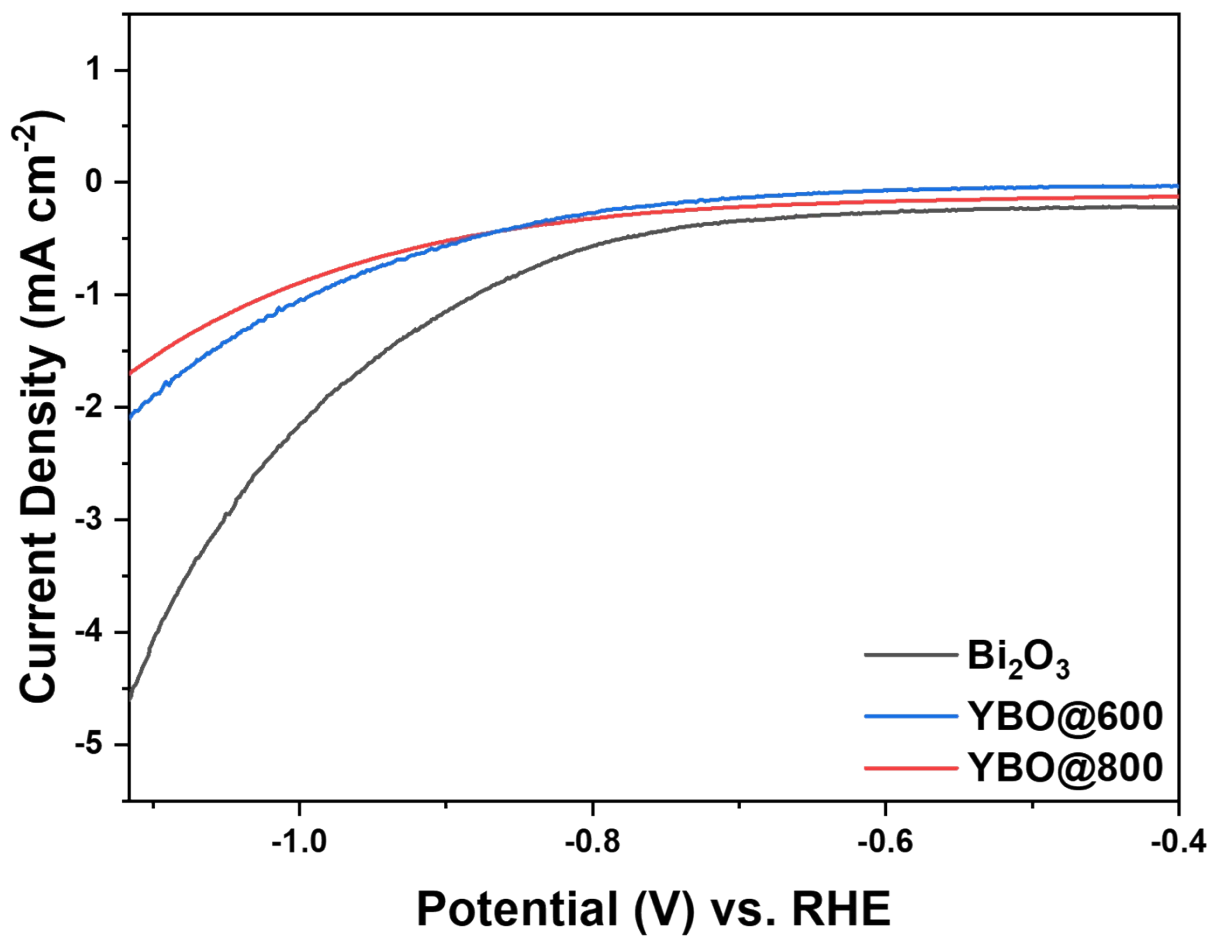


Fig. S3. LSV curves of Bi₂O₃ NPs, YBO@600 and YBO@800 in 0.1M KHCO₃ saturated with Ar.

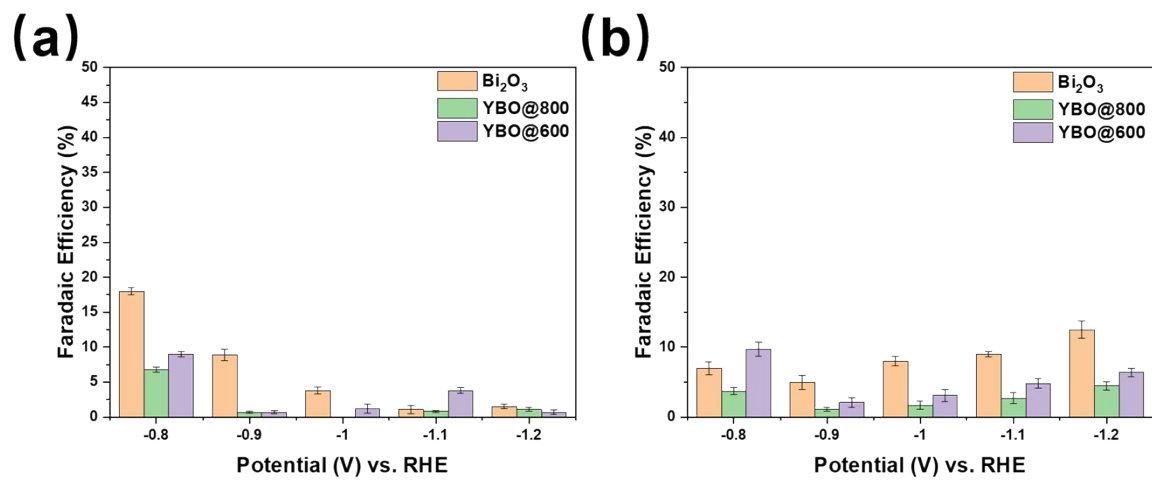


Fig. S4. (a) FE_{CO} diagram of Bi₂O₃ NPs, YBO@600 and YBO@800 at varied applied potentials. (b)

FE_{H_2} of Bi₂O₃ NPs, YBO@600 and YBO@800 at varied applied potentials.

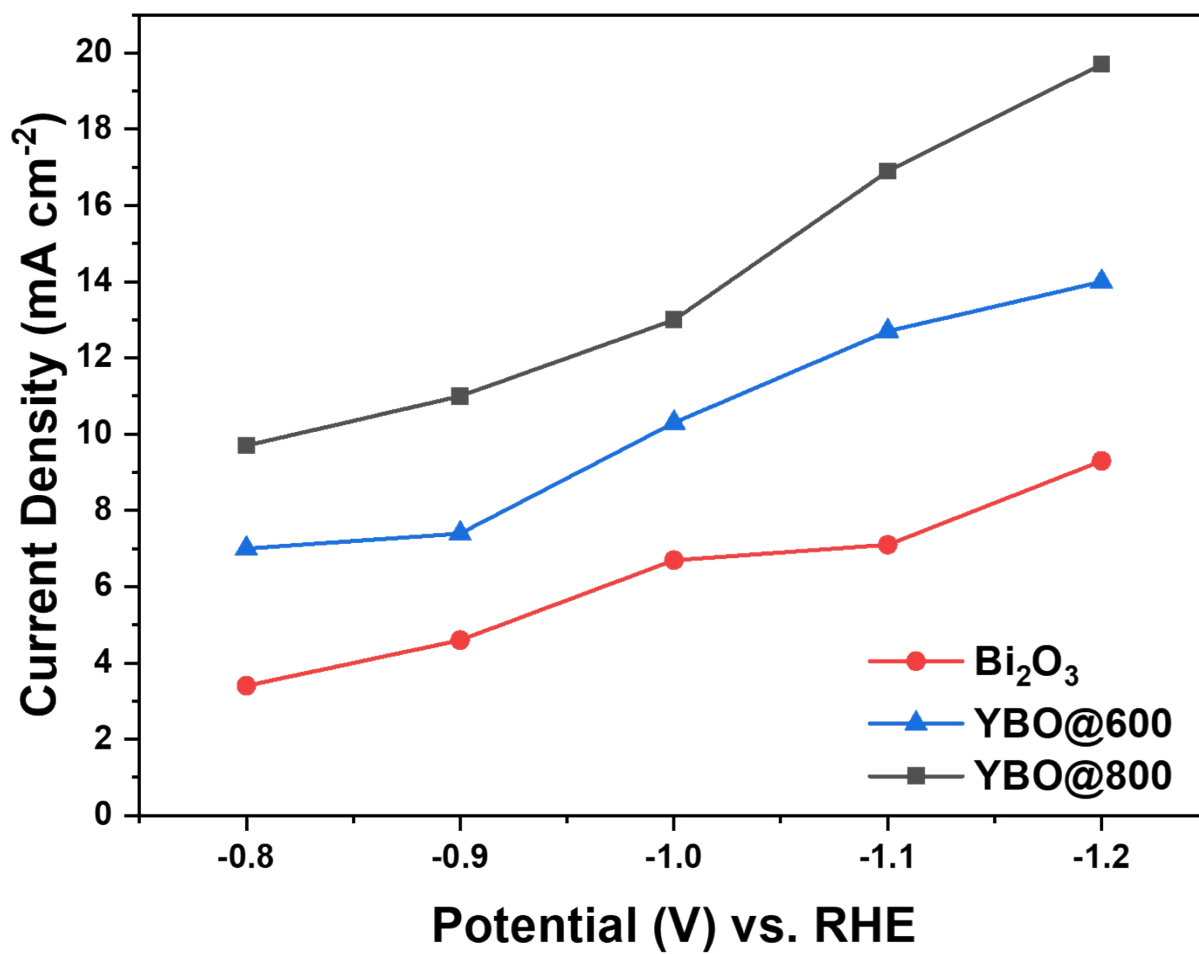


Fig. S5. Current density of Bi₂O₃ NPs, YBO@600 and YBO@800 at varied applied potentials.

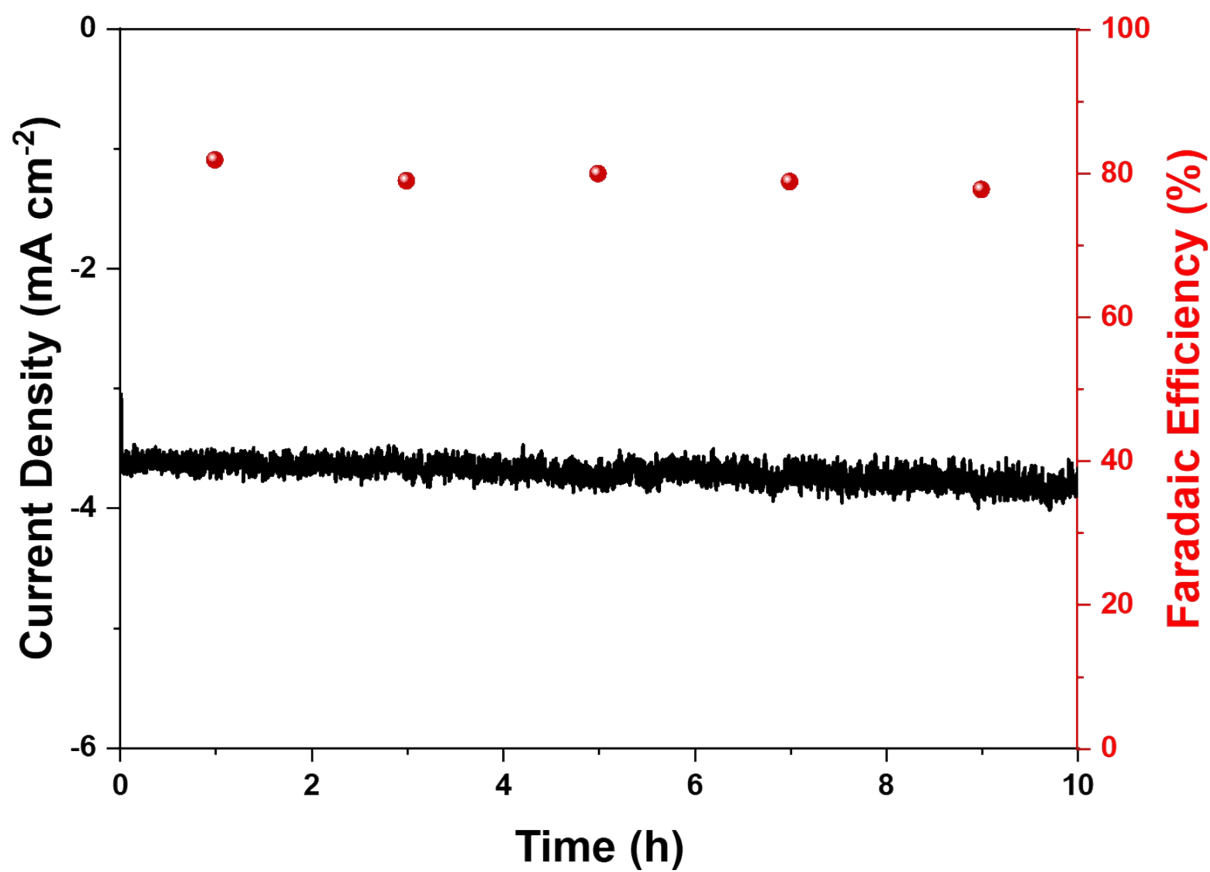


Fig. S6. The FE_{formate} and current density during the stability test of Bi_2O_3 NPs in H-type cell at $-0.9 V_{\text{RHE}}$.

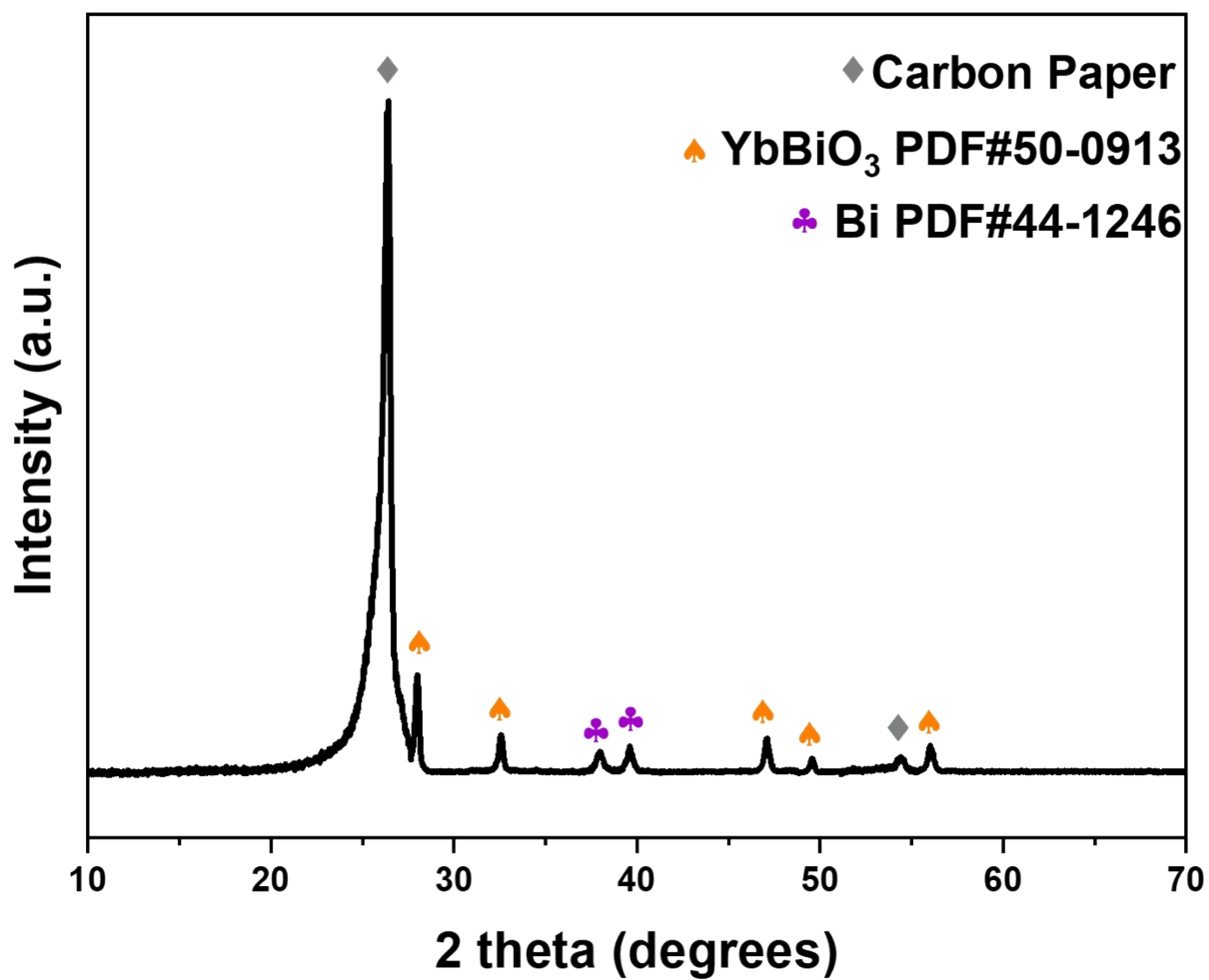


Fig. S7. XRD pattern of YBO@800 catalyst after 80h stability test.

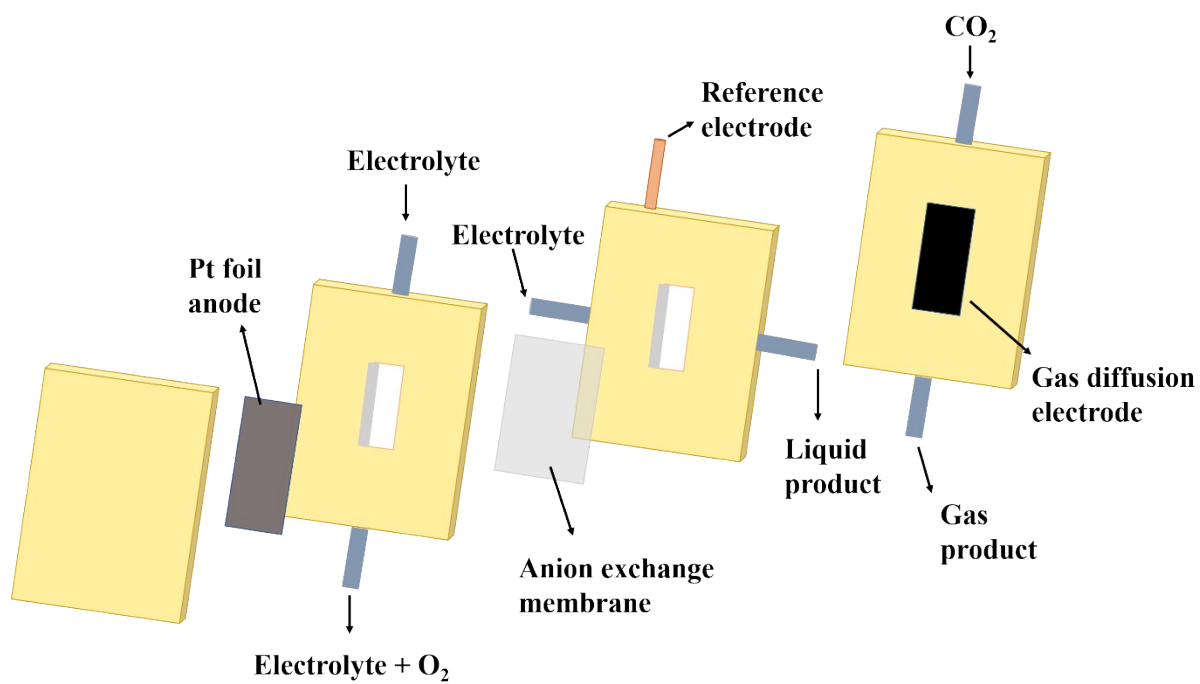


Fig. S8. Installation diagram of flow-cell.

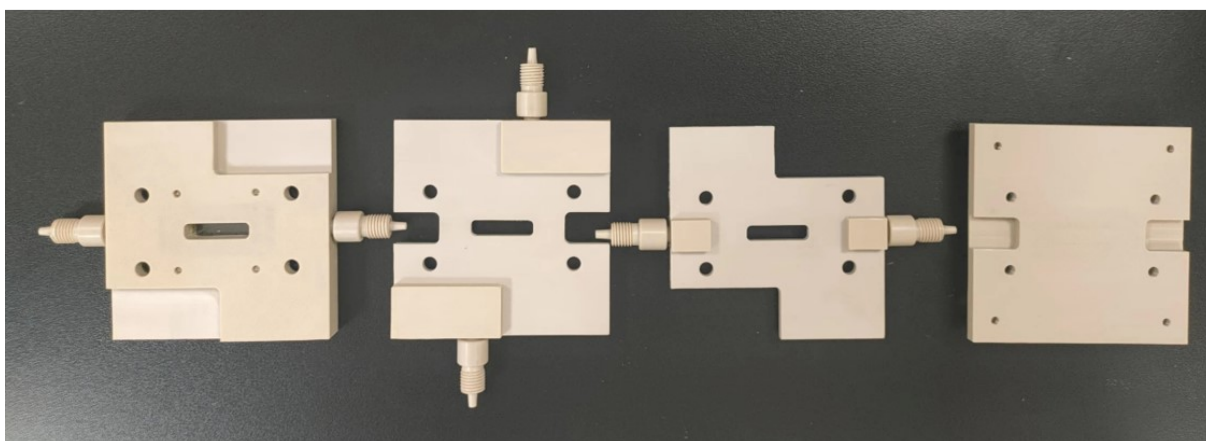
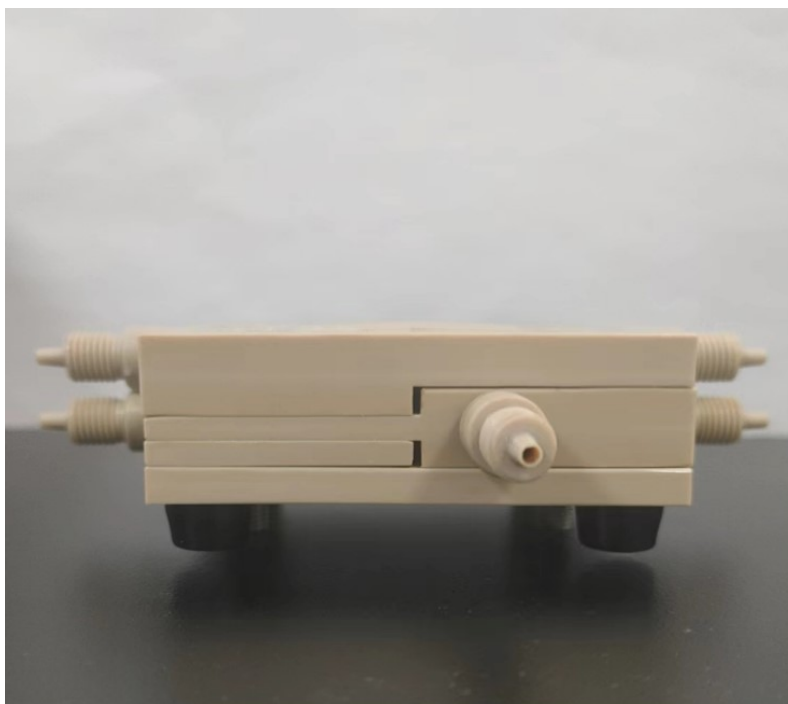


Fig. S9. Pictures of flow-cell system.

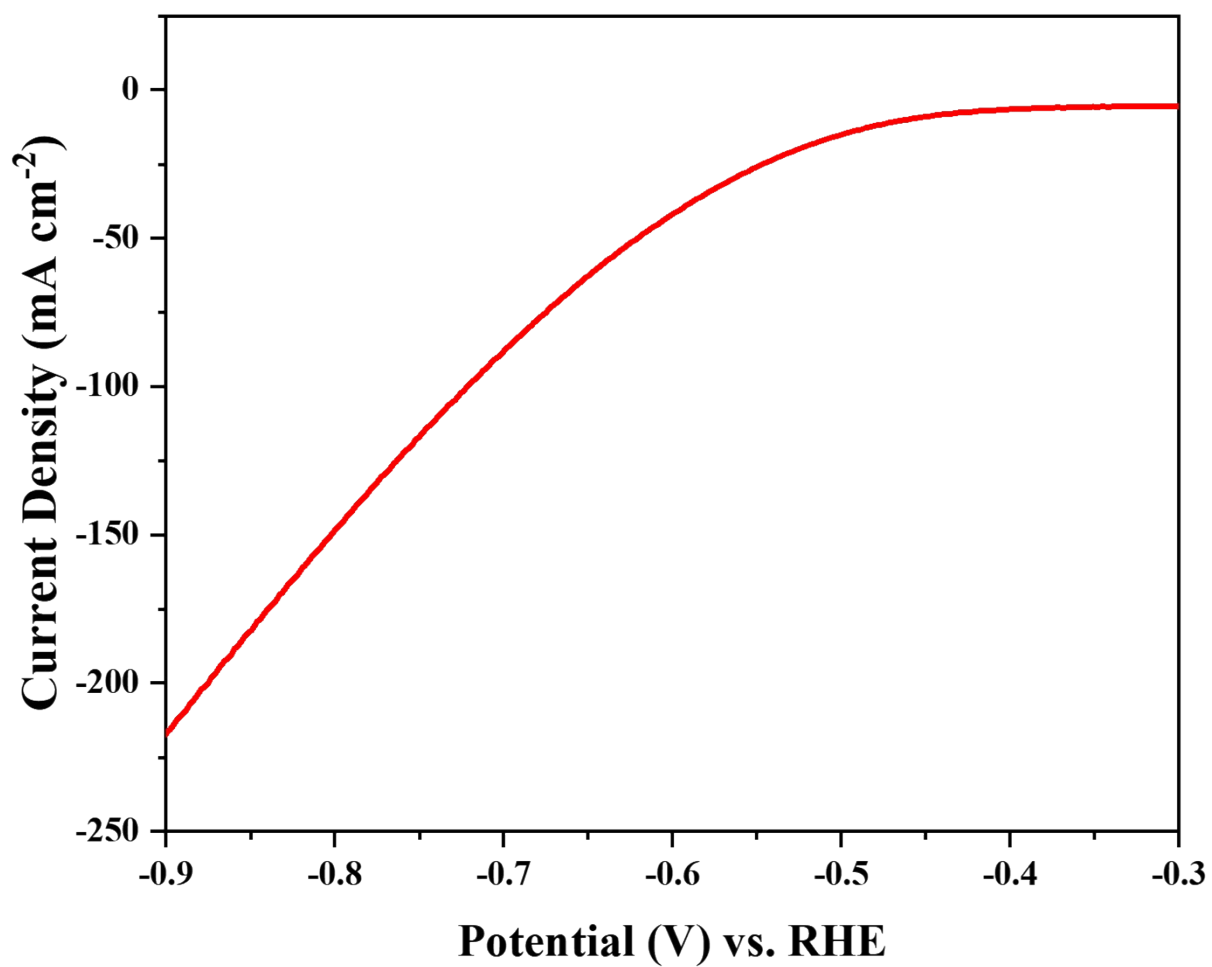


Fig. S10. LSV curve of the YBO@800 catalyst in the flow-cell with CO₂ injection.

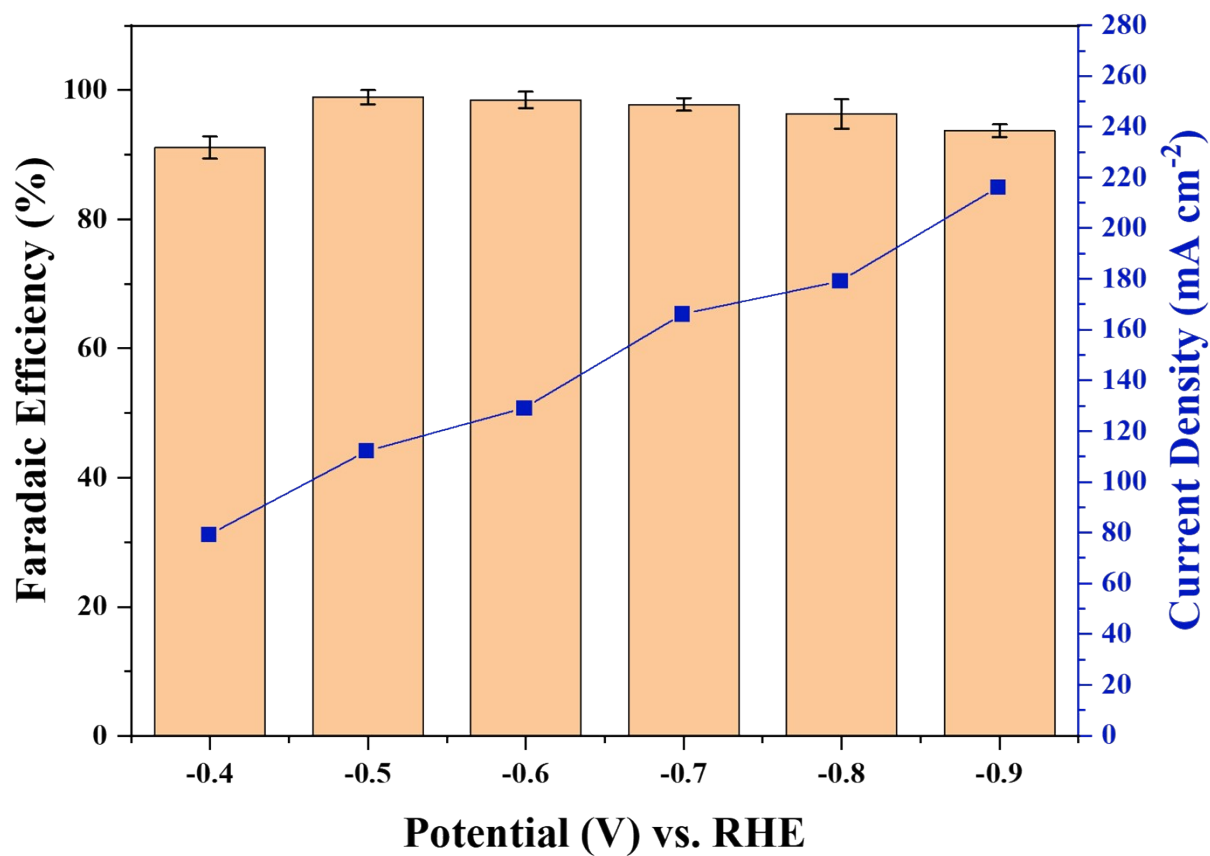


Fig. S11. The FE_{formate} and current density of the YBO@800 catalyst at different potentials in the flow-cell.

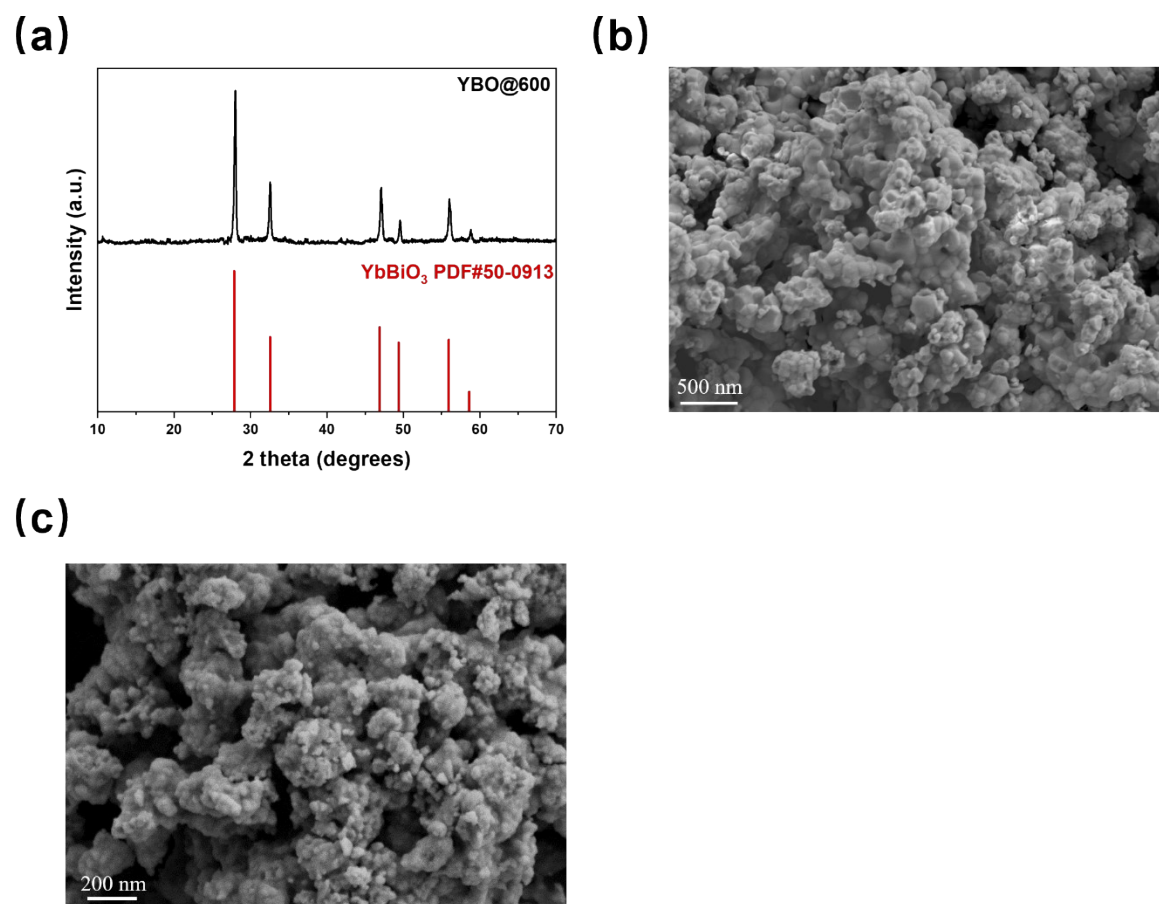
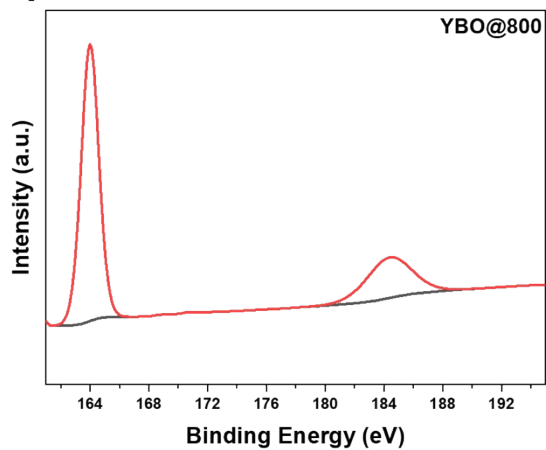


Fig. S12. (a) XRD pattern of YBO@600, SEM images of (b) YBO@600, (c) YBO@600 after electroreduction.

(a)



(b)

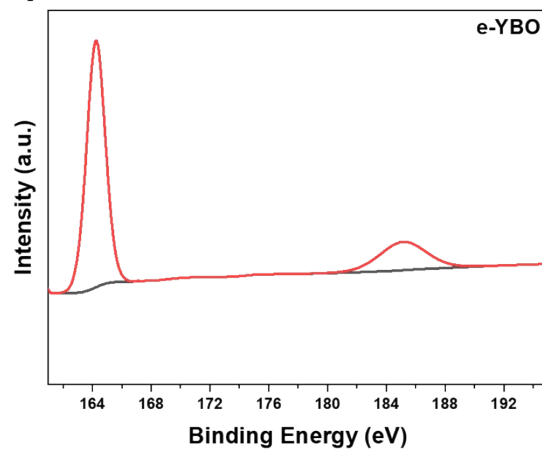


Fig. S13. Yb 4d XPS spectra of YBO@800 and e-YBO.

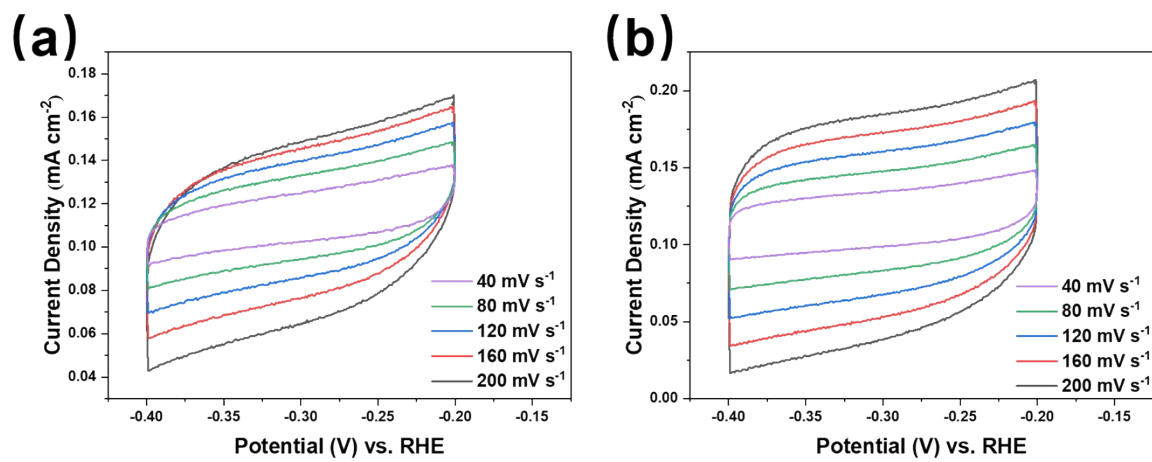


Fig. S14. CV curves of the catalysts at different sweep speeds: (a) YBO@800, (b) e-YBO.

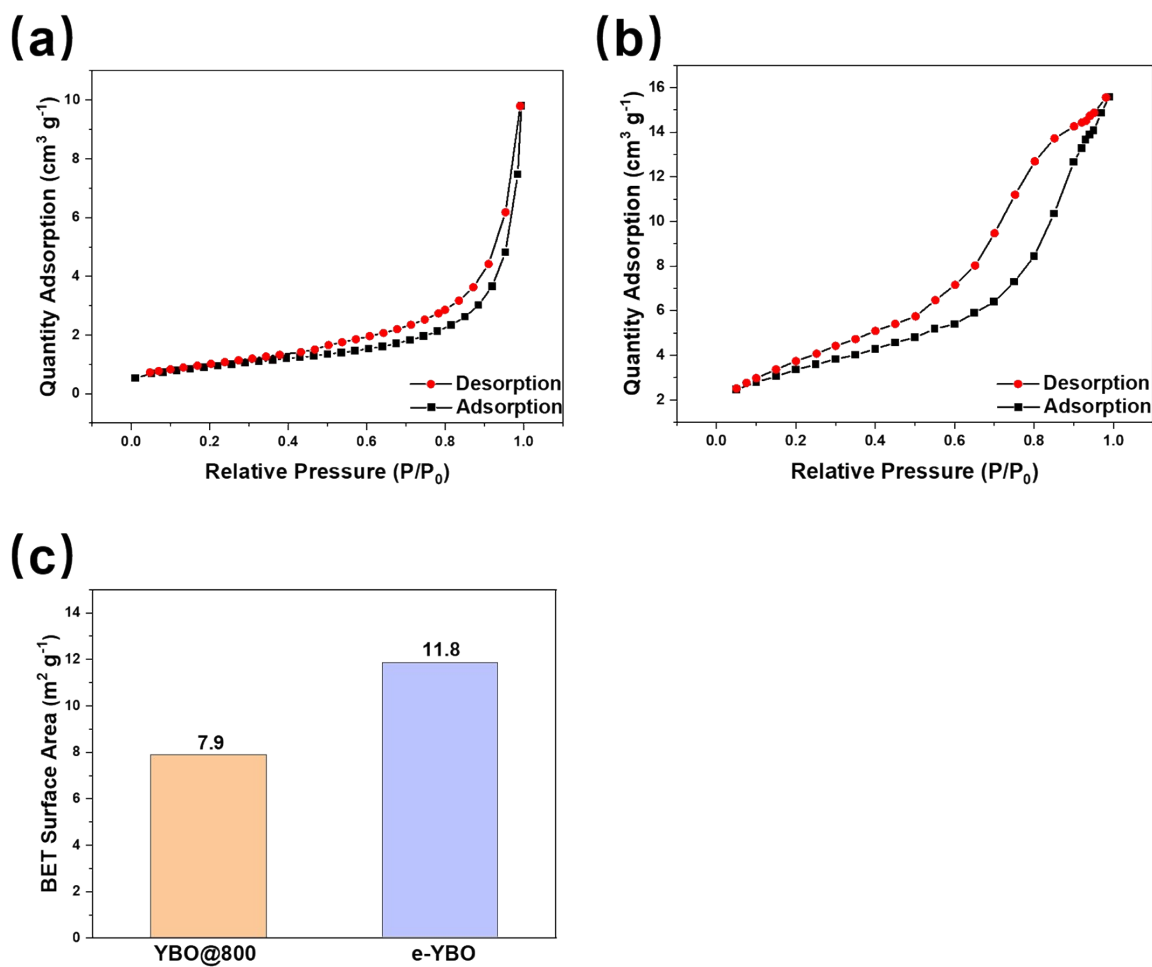


Fig. S15. (a) N₂ adsorption–desorption isotherms of YBO@800, (b) e-YBO. (c) BET surface area of YBO@800 and e-YBO.

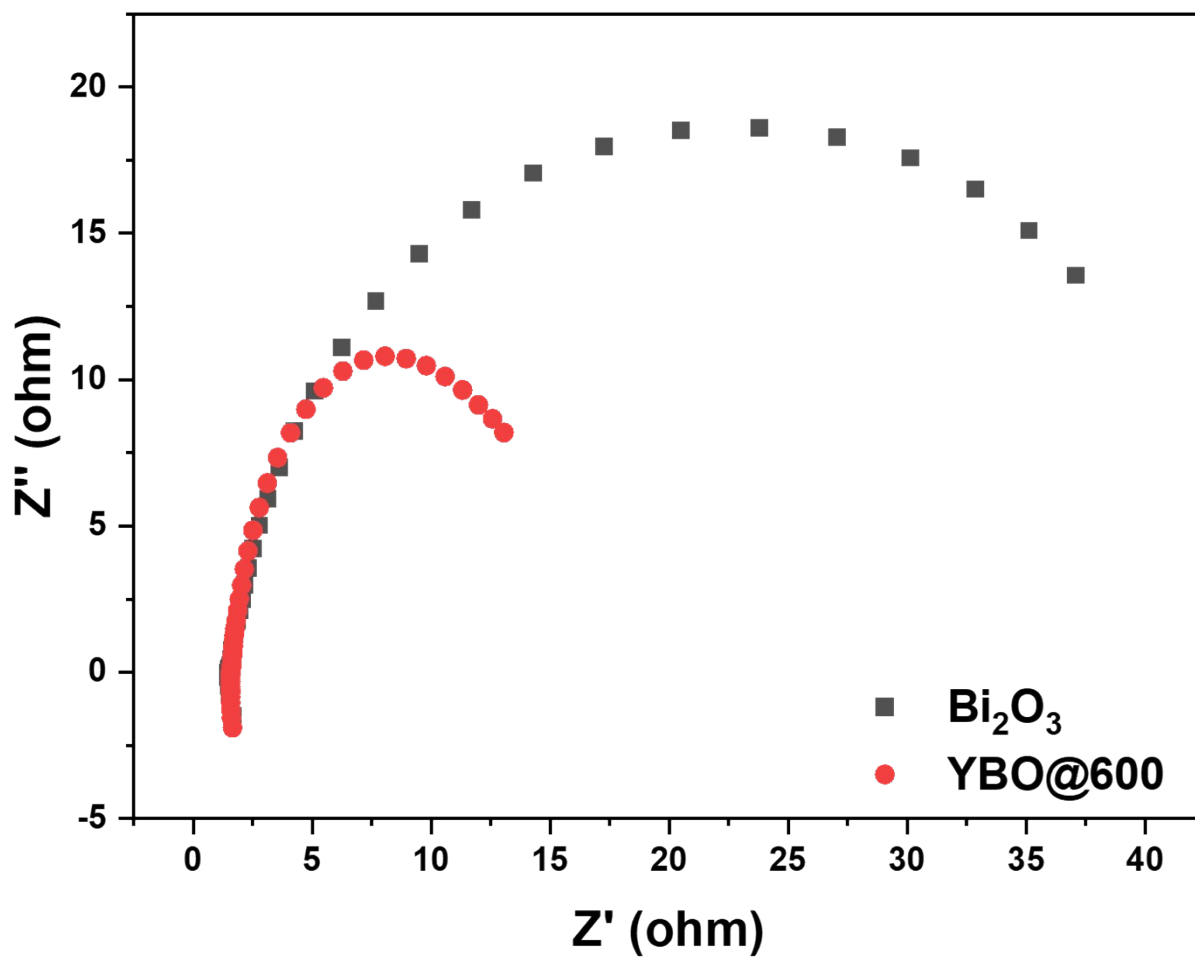


Fig. S16. EIS plots of Bi_2O_3 NPs and YBO@600.

Table. S1. Inductively Coupled Plasma Optical Emission Spectrometer (ICP-OES) results for mole ratio of Bi and Yb in YBO@800.

Sample	ICP-OES (mole ratio, Bi:Yb)
YBO@800	1:0.97